Received: 5 March 2024 | Revised: 18 June 2024 | Accepted: 21 June 2024

DOI: 10.1111/pce.15026

ORIGINAL ARTICLE

Plant, Cell & Environment | WILEY

Comparative proteomics analysis of root and nodule mitochondria of soybean

Wai-Ching Sin[1] | Jinhong Liu[2] | Jia Yi Zhong[2] | Hon-Ming Lam[1,3] | Boon Leong Lim[2,3]

[1]School of Life Sciences, The Chinese University of Hong Kong, Shatin, Hong Kong, China

[2]School of Biological Sciences, University of Hong Kong, Pokfulam, Hong Kong, China

[3]State Key Laboratory of Agrobiotechnology, The Chinese University of Hong Kong, Shatin, Hong Kong, China

Correspondence

Boon Leong Lim, School of Biological Sciences, University of Hong Kong, Pokfulam, Hong Kong, China.
Email: bllim@hku.hk

Hon-Ming Lam, School of Life Sciences, The Chinese University of Hong Kong, Shatin, Hong Kong, China.
Email: honming@cuhk.edu.hk

Funding information

Innovation and Technology Fund; Hong Kong Research Grants Council,
Grant/Award Number: AoE/M-403/16

Abstract

Legumes perform symbiotic nitrogen fixation through rhizobial bacteroids housed in specialised root nodules. The biochemical process is energy-intensive and consumes a huge carbon source to generate sufficient reducing power. To maintain the symbiosis, malate is supplied by legume nodules to bacteroids as their major carbon and energy source in return for ammonium ions and nitrogenous compounds. To sustain the carbon supply to bacteroids, nodule cells undergo drastic reorganisation of carbon metabolism. Here, a comprehensive quantitative comparison of the mitochondrial proteomes between root nodules and uninoculated roots was performed using data-independent acquisition proteomics, revealing the modulations in nodule mitochondrial proteins and pathways in response to carbon reallocation. Corroborated our findings with that from the literature, we believe nodules preferably allocate cytosolic phosphoenolpyruvates towards malate synthesis in lieu of pyruvate synthesis, and nodule mitochondria prefer malate over pyruvate as the primary source of NADH for ATP production. Moreover, the differential regulation of respiratory chain-associated proteins suggests that nodule mitochondria could enhance the efficiencies of complexes I and IV for ATP synthesis. This study highlighted a quantitative proteomic view of the mitochondrial adaptation in soybean nodules.

KEYWORDS

data-independent acquisition (DIA) proteomics, electron transport chain, *Glycine max*, legume, malate, nitrogen fixation, tricarboxylic acid cycle

1 | INTRODUCTION

Legumes such as soybean (*Glycine max*) can assimilate atmospheric nitrogen (N_2) into a bioavailable form (NH_4^+) by establishing symbiotic relationships with nitrogen-fixing rhizobia through specialised organs called root nodules (Liu et al., 2018). Nitrogen fixation by rhizobia is an energy-demanding process, with legume hosts providing carbon and energy sources to the nodule bacteroids to sustain the energy cost in rhizobia. Photoassimilates, mainly sucrose, are transported from shoots to nodules and converted into malate to provide the carbon source for rhizobia (Booth et al., 2021; Schulze et al., 2002). The symbiotic rhizobia in bacteroids then metabolise the

supplied malate to generate the energy required for the nitrogenase reaction that converts atmospheric nitrogen into ammonia and other nitrogenous compounds, which are transported back to the root cells of the host plant. The infected cells assimilate the received ammonium ions via nitrogen-assimilating enzymes, including glutamine synthetase (GS) and glutamine oxoglutarate aminotransferase/glutamate synthase (GOGAT). Some of the resulting glutamine would then enter the purine synthesis pathway and is eventually converted into ureides that are exported from the nodules to the whole plant (Liu et al., 2018).

In nodules, shoot-derived sucrose is the primary carbon source for energy metabolism. Sucrose is metabolised via the glycolysis pathway and subsequently converted to phosphoenolpyruvate (PEP) (Booth et al., 2021). Alternatively, sucrose can also be metabolised via the oxidative pentose phosphate pathway (OPPP) in plastids and in the cytosol to generate NADPH and ribose-5-phosphate (R5P) (Hong & Copeland, 1990; Kohl et al., 1990). PEP generated from glycolysis has two fates, either conversion into pyruvate by pyruvate kinases (PKs) of the glycolysis pathway, or conversion into oxaloacetate (OAA) by the action of phosphoenolpyruvate carboxylase (PEPC). Distinct from the situation in uninfected/uninoculated root tissues, where PEP is mainly used to generate pyruvate to feed the tricarboxylic acid (TCA) cycle in mitochondria to generate ATP, the glycolytic PEP in nodules is mainly destined for the synthesis of OAA rather than pyruvate (Ke et al., 2022; McCloud et al., 2001). Transcriptomic analyses of soybean nodules showed that the PEPC genes, *GmPEPC7* and *GmPEPC15*, were highly expressed in nodules (Wang et al., 2020). Consequently, PEP from the glycolytic pathway is converted into OAA via the activities of PEPCs, reducing the flux from PEP to pyruvate and to the TCA cycle in nodule mitochondria (Ke et al., 2022; McCloud et al., 2001). OAA is then reduced to malate by cytosolic malate dehydrogenase (MDH). The cytosolic OAA-to-malate conversion is specifically promoted in legume nodules. Such nodule-enhanced MDH (neMDH) activities can similarly be seen in the nodules of alfafa (*Medicago sativa*), pea (*Pisum sativum*), and *Lotus japonicus* (Fedorova et al., 1999; Miller et al., 1998; Takanashi et al., 2012). The cytosolic malate in nodules serves dual functions: it can either be exported to bacteroids or be transported into nodule mitochondria for NADH synthesis and subsequent ATP production via oxidation to OAA (Booth et al., 2021). It was found that soybean nodule mitochondria operate a modulated TCA cycle based on in vitro experiments, with increased malate oxidation activities, and decreased activities of malic enzymes (MEs) and other TCA cycle enzymes except MDH (Bryce & Day, 1990; Rawsthorne & Larue, 1986).

However, the carbon flux and energy metabolism inside nodule mitochondria remains an elusive topic. For instance, it was uncertain whether OAA is directly exported out of mitochondria or is first metabolised into other dicarboxylates. Therefore, it is critical for plant researchers to decipher the energy metabolism in nodules. While some reports addressed the proteomic changes in legume nodules, past studies of the nodule proteome either focused on the total proteomic changes only, or had limited coverage on mitochondrial proteins due to limitations in methodologies (Dam et al., 2014; Matamoros et al., 2013; Thal et al., 2018; Wang et al., 2022). As such, a comprehensive proteomic understanding of nodule mitochondrial adaptations to symbiotic nitrogen fixation is currently lacking. To delineate the roles of mitochondria in nodule metabolism in the present study, we performed a quantitative data-independent acquisition (DIA)-based mitochondrial proteomic comparison on soybean nodules versus uninoculated roots. Our result revealed specific adaptations by nodule mitochondria in energy metabolism and the role of nodule mitochondrial proteins in N-assimilation. To mediate the N-assimilation process, the nodule adopts an alternative carbon metabolic pathway for ATP synthesis and N-assimilation. This analysis thus provides a proteomic blueprint of mitochondrial adaptations in symbiotic soybean nodules.

2 | MATERIALS AND METHODS

2.1 | Plant materials and rhizobial inoculation

Cultivated soybean C08 (*G. max*), which is closely related to Williams 82 from Illinois, USA, was used for nodule harvesting in this experiment. At 3 days postgermination, plants were inoculated with *Sinorhizobium Fredii* strain CCBAU45436. A group of uninoculated soybeans for root tissue harvest were grown alongside the inoculated soybeans under the same conditions. Plant growth and inoculation conditions were performed as described previously (Sun et al., 2020). A total of five biological replicates were performed on both the uninoculated root and nodule groups.

2.2 | Mitochondrion isolation and protein extraction

At 28 days postinoculation (DPI), uninoculated root and nodule tissues were harvested separately and flash-frozen in liquid nitrogen. Soybean mitochondria from uninoculated roots and nodules were subsequently isolated via a sucrose and Percoll density gradient as described in a previous work (Sun et al., 2020). Isolated mitochondria were transferred to 2-mL centrifuge tubes in a 0.7 M sucrose homogenisation buffer. Two stainless steel beads were added to each tube and the mitochondrial samples were homogenised with a tissue homogeniser for 2 min. After removing the beads, two volumes of phenol equilibrated with Tris-HCl, pH 8.0, were added to each of the homogenates, and mixed by shaking for 15 min. The mixtures were centrifuged at 25 000 *g* at 4°C for 15 min. The top phenol phase was collected, transferred to 10-mL centrifuge tubes, and precipitated with 5 volumes of ice-cold methanol buffer (0.1 M ammonium acetate, 10 mM DTT) at −20°C for 2 h. The protein pellets were collected by centrifugation at 25 000 *g* at 4°C for 15 min and the supernatants were discarded. The protein pellets were then washed twice with ice-cold methanol buffer, with each wash being followed by centrifugation at 25 000 *g* at 4°C for 15 min. After the washes, the

protein pellets were incubated with ice-cold acetone at −20°C for 30 min. The protein pellets were then collected by centrifugation at 25 000 *g* at 4°C for 15 min and the supernatants were discarded. The acetone precipitation step was repeated once.

2.3 | Protein digestion

Protein pellets were air-dried and then solubilized in lysis buffer (1% SDS, 10 mM dithiothreitol [DTT], 50 mM NH_4HCO_3). After centrifugation at 25 000 *g* at 4°C for 15 min, the supernatants were transferred to new tubes and put into a 56°C water bath for 1 h. After cooling down to room temperature, the reduced protein samples were alkylated by 55 mM iodoacetamide for 45 min in the dark. Protein samples were precipitated again with 5 volumes of acetone at −20°C for 2 h. The protein pellets were collected by centrifugation at 25 000 *g* at 4°C for 15 min. Then, the proteins were resuspended in lysis buffer without SDS. Before protein digestion, the protein concentrations were quantified by the Bradford method. Ten micrograms of each protein sample were aliquoted for SDS-PAGE to confirm sample quality before proceeding to digestion. Then 100 µg was aliquoted from each protein sample replicate and diluted with 4 volumes of 50 mM NH_4HCO_3. Trypsin digestion was performed with an enzyme-to-protein ratio of 1:40 for 4 h at 37°C. Digested samples were desalted with Strata X column (Phenomenex) and peptide eluates were dried in vacuo. The dried samples were then resuspended in 2% acetonitrile (ACN) with 0.1% formic acid (FA) before downstream analyses.

2.4 | Nanoflow liquid chromatography-tandem mass spectrometry (LC–MS/MS) analysis

Mass spectrometry proteomic analyses were conducted by Beijing Genomic Institute (BGI). For both data-dependent acquisition (DDA) and DIA analyses, peptide samples were analysed using the mass spectrometer Oritrap Exploris 480 (Thermo Fisher Scientific), in positive ion mode with an ion spray voltage of 1900 V in both acquisition modes. The default charge state was set to 2. Peptide injections were carried out by the Thermo UltiMate 3000 UHPLC liquid chromatography system (Thermo Fisher Scientific) and separation was performed on a self-packed C18 column (150 µm internal diameter, 1.8 µm column size, 35 cm column length) operating at a flow rate of 500 nL min^{-1}.

For DDA analyses, equal amounts of peptides from all samples were aliquoted and pooled into one sample for basic-pH RPLC (bRPLC). The pooled sample was diluted in solvent A (5% ACN, pH 9.8) and injected into the Shimadzu LC-20AB HPLC system (Shimadzu Corporation, Japan) coupled with a Gemini high-pH C18 column (5 µm, 4.6 × 250 mm; Phenomenex). The sample was loaded onto the column and eluted, at a flow rate of 1 mL min^{-1}, with the following gradient: 5% solvent B (95% ACN, pH 9.8) for 10 min, 5% to 35% solvent B for 40 min, 35%–95% solvent B for 1 min, 95%–5% solvent B for 3 min and 5% solvent B equilibration for 10 min. The elution peak was monitored at 214 nm and the components were collected at 1-min intervals. The collected components were combined into 10 fractions in total, which were then freeze-dried.

Dried peptide fractions were resolubilized in solvent A (2% ACN, 0.1% FA) and injected into the UHPLC system. Samples were collected with a linear gradient from 5% to 25% solvent B (98% ACN, 0.1% FA) for 115 min, and then from 25% to 35% solvent B for 40 min before tandem mass spectrometry. MS1 survey scans in the 350–1650 mass-to-charge (*m/z*) range were acquired at a resolution of 120 000, maximal injection time (MIT) of 90 ms, and normalised auto gain control (AGC) target of 300%. The top 30 precursors with a charge state of 2+ to 6+ and an intensity over $2e^4$ were selected for tandem MS. MS2 spectra were acquired with the orbitrap at a resolution of 30 000, an isolation window of 1.6 *m/z*, MIT in 'auto' setting, a dynamic exclusion time of 120 s, normalised AGC target of 100%, collision type in higher-energy collisional dissociation (HCD), and normalised collision energy (NCE) at 30%.

For DIA single-injection analyses, individual samples were first separated on the above-mentioned UHPLC system with a linear gradient from 5% to 25% solvent B for 85 min, and then from 25% to 35% solvent B for 10 min before tandem mass spectrometry. MS1 survey scans in the 400–1250 *m/z* range were acquired before every MS2 scan cycle at a resolution of 120 000, MIT of 90 ms, and normalised AGC target of 300%. MS2 scans were performed with 50 isolation windows with a 1-*m/z* overlapping window covering a 400–1250 *m/z* range. MS2 spectra were acquired with the orbitrap at a resolution of 30 000, MIT in 'auto' setting, normalised AGC target of 1000%, collision type in HCD, and NCE at 30%.

2.5 | Mass spectrometry data analysis

Mass spectrometry data analyses were performed by the BGI bioinformatic analysis pipeline. DDA mass spectrometry data were first analysed using the Andromeda search engine in MaxQuant (v1.5.3.30) to search against the soybean cultivar William 82 protein sequence database (Wm82.a4.v1) for peptide and protein identifications (Tyanova et al., 2016). The following parameters were used in the database search: trypsin digestion; minimum peptide length of 7 aa; cysteine carbamidomethylation as fixed modification; methionine oxidation and N-terminal acetylation as variable modifications; and false discovery rate (FDR) filter of 1% at the peptide and protein levels. The DIA mass spectrometry data were processed by a BGI in-house software implemented with the mProphet algorithm (Reiter et al., 2011). MaxQuant results were used as the spectral library for peptide and protein identifications. Based on the target-decoy model, false positive control was performed with FDR set at 1%. Quantified protein abundance values were obtained from individual runs for downstream analyses.

The identified proteins were searched against the NCBI and Swiss-Prot databases for protein homology, and against gene ontology (GO) and EuKaryotic Orthologous Groups (KOG) for

functional annotations. Subcellular localisation predictions of identified protein sequences were performed using the TargetP-2.0 and DeepLoc-2.0 prediction models available on services.healthtech.dtu.dk (accessed on 2023/9/21) (Almagro Armenteros et al., 2019; Thumuluri et al., 2022). With DeepLoc-2.0, subcellular localisation was determined by the subcellular compartment with the top probability score. The mass spectrometry proteomics data have been deposited to the ProteomeXchange Consortium via the PRIDE partner repository with the data set identifier PXD050301 (Deutsch et al., 2023; Perez-Riverol et al., 2022).

2.6 | Quantitative analysis

Proteins quantified in four or five replicates in one tissue group and had zero detection in another group were marked as 'tissue-unique proteins'. For relative quantification analyses, tissue-unique proteins were discarded and only those proteins which were identified in all five replicates in both root and nodule were retained. Differential protein expression was determined by pairwise comparisons of normalised protein abundances between groups using the Bioconductor R packages, edgeR and LIMMA (Ritchie et al., 2015; Robinson et al., 2010). The protein abundance values were renormalized in edgeR using the 'TMM' normalisation method, assuming the majority of the proteins are not differentially expressed across tissue groups. The statistical test was performed in LIMMA, which fits a linear model to the protein abundance data to provide a high quantitative fidelity in DIA data analyses (Dowell et al., 2021). Quantified proteins with |fold-change (FC)| > 2 and adjusted $p < 0.05$ were marked as differentially expressed proteins (DEPs).

For relative protein abundance estimations, only those proteins that were detected in all five replicates in each tissue group were included. Individual protein intensities were divided by the summed protein intensity to obtain relative protein abundances. The averaged relative protein abundance values among all five replicates were sorted by subcellular localisation predictions to decipher the proteome composition of each tissue group. Correlation analyses were performed in R using the *cor* function which uses the Pearson method. Principal component analysis (PCA) was performed in R using the *prcomp* function. Plots for data visualisation were generated in R using the *ggplot2* packages.

2.7 | Validation of proteomics data by Western blot analysis

One and 2 μg each of another batch of soybean mitochondrial proteins extracted from uninoculated roots or nodules were separated on 10% (w/v) SDS-PAGE and blotted on nitrocellulose membranes. The blots were blocked with 5% (w/v) nonfatty milk in TBST buffer (1 × TBS, 0.1% [v/v] Tween 20) for 1 h, followed by three 5-min washes with TBST. Then blots were incubated with 1:4000 anti-beta subunit of ATP synthase polyclonal antibodies (ATPβ; Agrisera, AS05085), 1:5000 anti-serine hydroxymethyltransferase polyclonal antibodies (SHMT; Agrisera, AS05075), 1:1000 anti-plant alternative oxidase 1 and 2 polyclonal antibodies (AOX; Agrisera, AS04054), 1:5000 anti-isocitrate dehydrogenase polyclonal antibodies (IDH; Agrisera, AS06203A), 1:1000 anti-mitochondrial NAD-dependent ME polyclonal antibodies (NAD-ME, Agrisera, AS163932), 1:10 000 anti-Tom40 polyclonal antibodies at 4°C overnight (Duncan et al., 2011), followed by a 1-h incubation with 1:40 000 secondary goat anti-rabbit horseradish peroxidase HRP-coupled antibodies (Agrisera, A509602). Blots were then visualised with chemiluminescent HRP substrates (aZURE; AC2204).

3 | RESULTS

3.1 | Quantitative comparisons between soybean root and nodule mitochondrial proteomes

After isolating mitochondrial proteins from tissues of uninoculated root and nodule, we first performed an initial DDA-based proteome analysis on pooled samples from both tissue groups for peptide and protein identification. To increase the proteome coverage, the pooled peptide samples were fractionated into 10 fractions by bRPLC before LC–MS/MS. The MS spectra were processed by the MaxQuant software for peptide identification. In total, 6050 proteins were identified in our initial mitochondrial proteome library (Figure 1, Supporting Information: Table S1).

To observe any biological differences between mitochondrial proteomes, it is of particular importance to first differentiate mitochondrial proteins from nonmitochondrial ones. To predict subcellular localisations, identified protein sequences were analysed by DeepLoc2.0, a subcellular protein localisation prediction tool (Thumuluri et al., 2022). Results showed that mitochondrial proteins were the most numerous category among the identified proteins, with up to 1203 proteins (Figure 2a).

Single-injection DIA proteomic analyses were then performed on each replicate, and the protein abundances of individual runs were quantified (Figure 1, Supporting Information: Table S1). The measured protein abundances were again analysed by DeepLoc2.0 for subcellular localisation predictions (Supporting Information: Table S1). Up to 66.5% and 70.9% of the total protein abundances were predicted to have originated from the mitochondria in nodule and uninoculated root samples, respectively (Figure 2b). Comparing individual protein abundances, the mitochondrial proteins were found to be enriched by up to 10 folds over nonmitochondrial proteins in both nodule and root samples (Figure 2c,d). These results indicated a successful enrichment of mitochondrial proteins in our extraction process. When examining tissue-specificity, 188 of the quantified proteins were uniquely found in nodule tissues, with 17 of them predicted to be localised in the mitochondrion (Supporting Information: Table S2). On the other hand, 689 of the identified proteins were unique to root tissues, but only 18 of them were predicted to be mitochondrially localised (Supporting Information: Table S3).

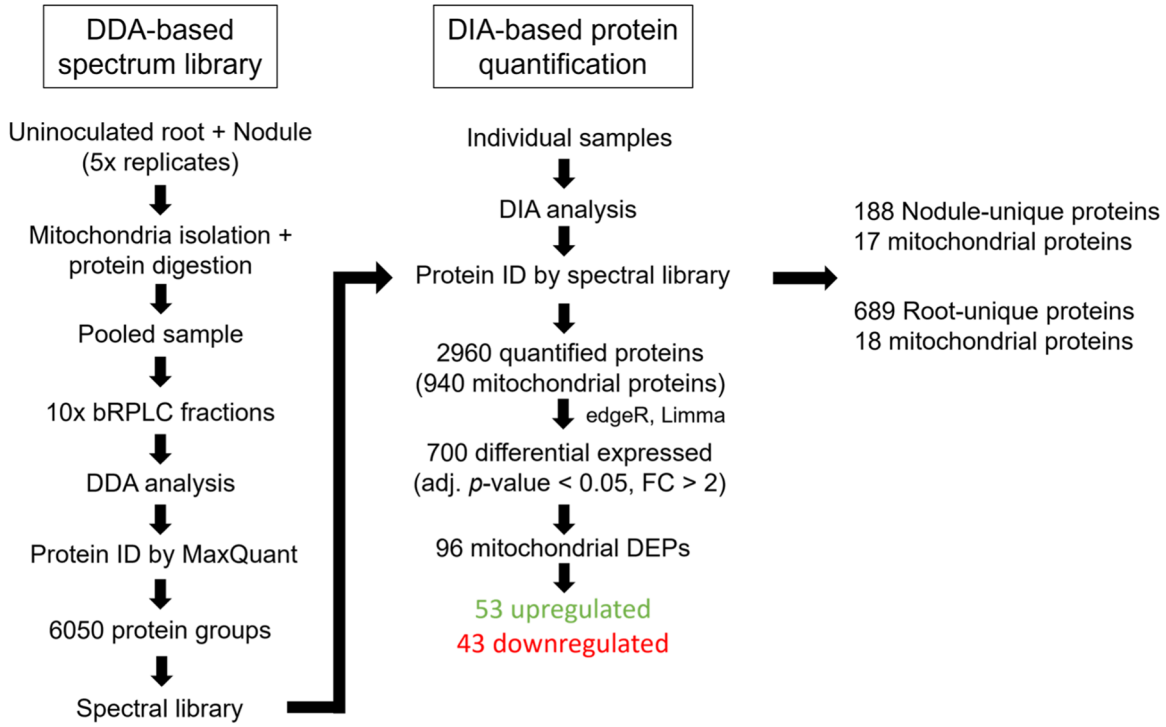

FIGURE 1 Proteomic workflow for data-dependent acquisition (DDA) spectral library preparation and data-independent acquisition (DIA) quantification of the nodule mitochondrial proteome. [Color figure can be viewed at wileyonlinelibrary.com]

The subcellular localisations of tissue-unique proteins revealed some issues with tissue-specific contaminations, where nodule mitochondrial extracts were prone to plastidic contaminants while those from root samples tended to be contaminated with cytosolic proteins.

Although the protocols for plant mitochondrion isolation have been optimised over the years to minimise contaminations from other organelles (Day et al., 1985; Sun et al., 2020), the combination of off-line fractionated DDA proteome identification and the unbiased nature of DIA quantification may have greatly enhanced the signals of low-abundance contaminant proteins, revealing the technical difficulties in achieving pure plant mitochondrion isolation (Rugen et al., 2023). Moreover, dual-targeting proteins are an evolutionarily conserved phenomenon in eukaryotic cells, where some proteins can be localised to more than one cellular compartment and therefore are beyond the capability of current prediction tools (Carrie & Small, 2013; Kisslov et al., 2014; Voon et al., 2021). We also could not exclude the possibility of contaminants originating from protein interactions on the mitochondrial membrane. It is possible that some of the predicted nonmitochondrial proteins were colocalized on the mitochondrial membrane through interactions with mitochondrial proteins, and hence ended up in the mitochondrial extract. Despite these constraints, on the basis of measured protein abundances, the intragroup proteomic results were highly consistent among replicates with Pearson correlation coefficients >0.90 (Figure 3a), and the nodule and uninoculated root sample groups were distinct from each other, based on PCA (Figure 3b). Such results indicated the technical consistency of mitochondrion isolation in our experiment despite unavoidable tissue-specific contaminants.

For pairwise tissue comparisons, only those proteins present in all samples were retained for renormalisation and no data imputation was applied. In the final data set, 2960 proteins were quantified, with 940 predicted mitochondrial proteins among them (Figure 4a, Supporting Information: Table S4). Based on statistical analysis using LIMMA, 700 proteins were shown to be differentially expressed (adjusted p-value < 0.05, $|FC| > 2$) (Figure 4b). However, as already mentioned, some tissue-specific low-abundance contaminants were observed in both sample groups (Figure 2e,f), and therefore the data have to be carefully interpreted. The analysis of protein FC distributions showed that the renormalized data were concentrated around mitochondrial proteins, but the plastidic and peroxisomal fractions were also shown to be present, mostly in the nodule, while cytoplasmic fractions were concentrated in the root (Figure 4c). This reflects the tissue-specific differences in subcellular localisations of the initial extracts. Based on the distribution pattern of mitochondrial proteins while assuming that most of them remained unchanged across tissue types, our data analysis strategy should be able to reflect the actual biological differences in the mitochondrial proteomes between tissue groups. Still, for nonmitochondrial proteins, except those supported by literature to be mitochondrially localised or mitochondrion-associated, the quantitative results would not be considered biologically significant. However, to demonstrate

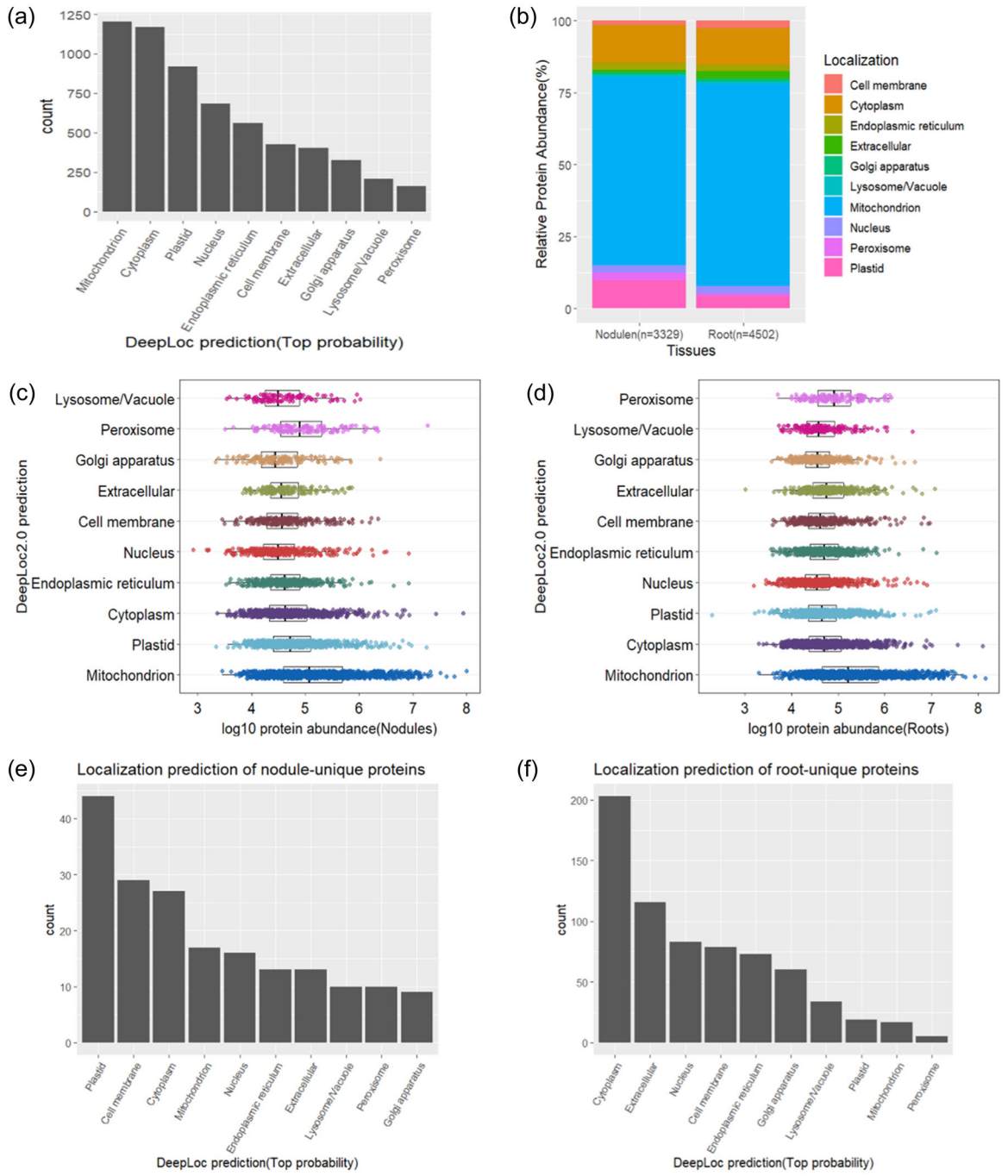

FIGURE 2 Qualitative assessment of the nodule and root mitochondrial proteome identifications. (a) Subcellular localisation prediction (DeepLoc2.0, top probability) of total identified proteins. (b) Relative protein abundance (in % total mass spectrometry [MS] intensity) in each tissue group. Only proteins identified in all five replicates were included. (c–d) Dynamic range of protein quantities in the nodule (c) and root (d) mitochondrial proteomes (MS intensity-based, arbitrary unit). The subcellular localisation predictions were sorted by the number of proteins in each category. (e–f) Subcellular localisation predictions of (e) nodule- and (f) root-unique proteins. [Color figure can be viewed at wileyonlinelibrary.com]

the completeness of our data, all nonmitochondrial proteins were reported. Ultimately, 95 mitochondrial proteins were found to be significantly up/downregulated in the soybean nodule compared to the uninoculated root, with 53 of them significantly induced and 42 significantly repressed (Figure 4d).

3.2 | Soybean nodule mitochondria prefer malate over pyruvate as the major source of reducing power

The expressions of mitochondrial proteins controlling the flux of the TCA cycle were significantly altered in soybean nodules (Table 1).

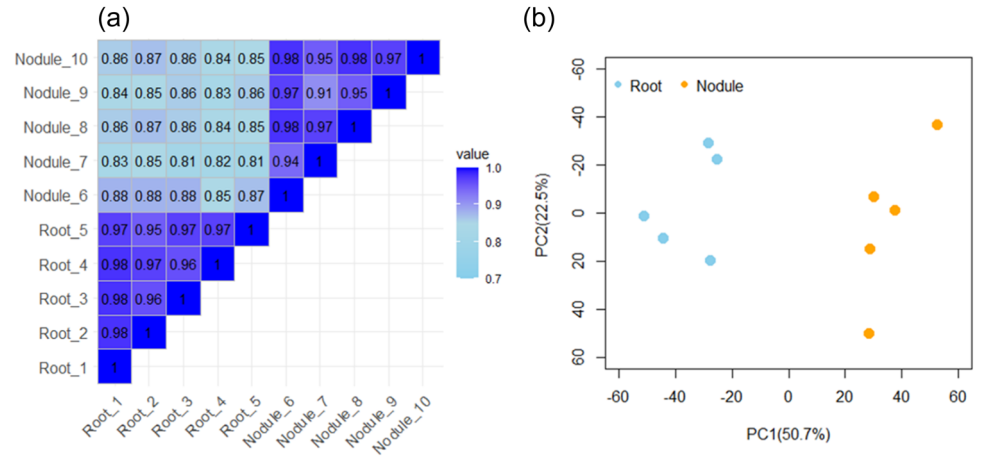

FIGURE 3 Evaluation of the technical consistency of mitochondrial proteome analyses. (a) Pearson correlation matrix of protein quantities in all replicates. Root_1 to Root_5 are five independent inoculated root mitochondrial samples. Nodule_6 to Nodule_10 are five independent nodule mitochondrial samples. (b) Principal component analysis (PCA) of root and nodule mitochondrial proteomes. All quantified proteins were included in the PCA analysis ($n = 2960$). [Color figure can be viewed at wileyonlinelibrary.com]

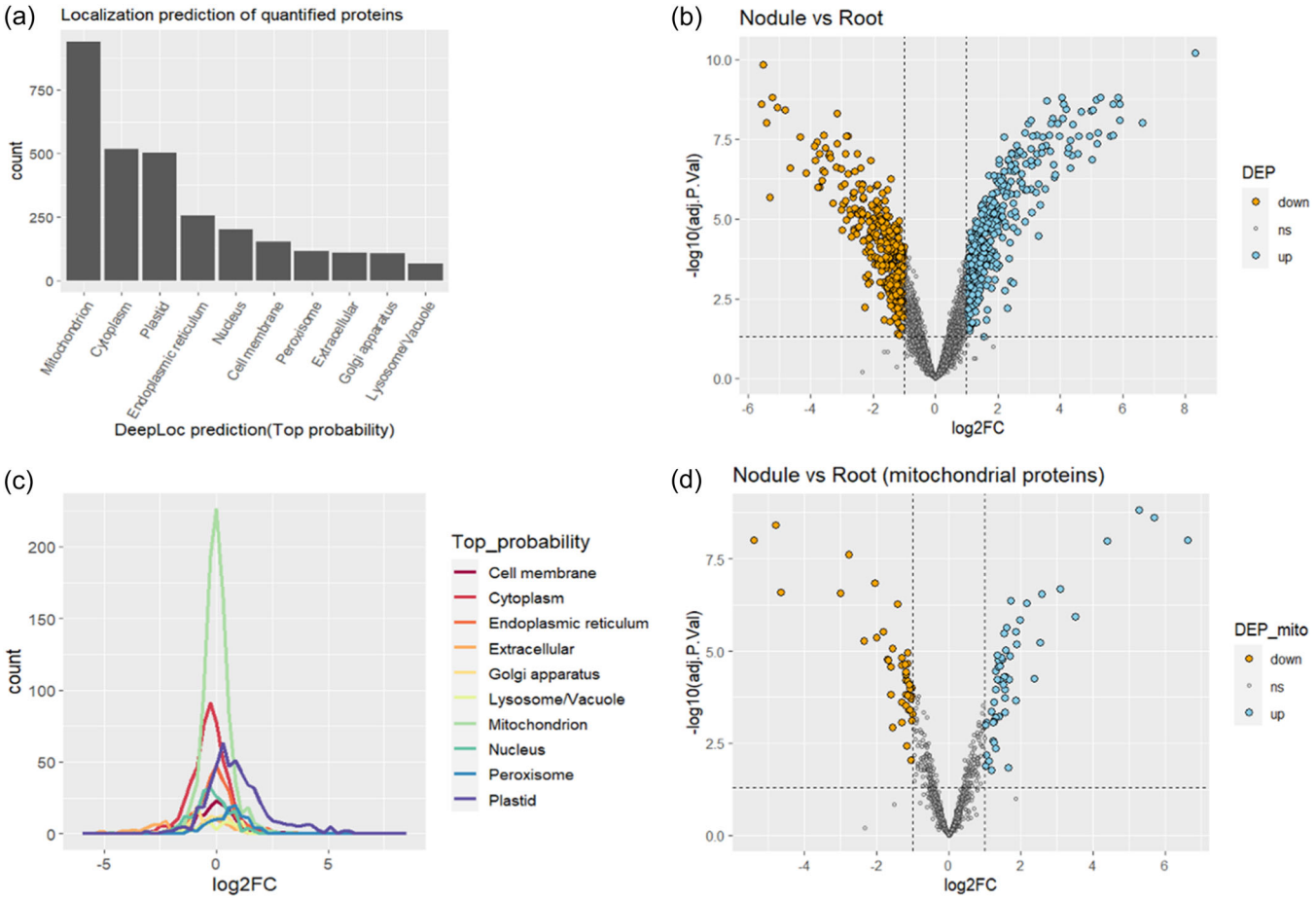

FIGURE 4 Quantification of nodule and root mitochondrial proteomes. A total of 2960 proteins were quantified. (a) Subcellular localisation predictions of quantified proteins (DeepLoc 2.0, top probability). (b) Volcano plot for visualising the quantitative comparison between the nodule and root mitochondrial proteomes. Differentially expressed proteins (DEPs) were coloured ($\log_2$FC > 1 and adjusted $p < 0.05$). (c) Log_2 fold-change (FC) distributions of the quantified proteins categorised according to their subcellular localisation predictions. (d) Volcano plot for visualising the quantitative comparison between the nodule and root mitochondrial proteomes, focusing on the mitochondrion-localised proteins only ($n = 940$). Orange, downregulated; blue, upregulated; ns, not significant; FC, fold-change. [Color figure can be viewed at wileyonlinelibrary.com]

TABLE 1 Differentially expressed mitochondrial proteins involved in the TCA cycle.

Protein_ID	Log_2FC	Adj. *p*-value	Differential expression	Protein description
Glyma.09G079000.1	1.716	4.40E−07	up	Pyruvate dehydrogenase [lipoamide] kinase-like
Glyma.15G188500.1	1.534	5.04E−05	up	Pyruvate dehydrogenase (acetyl-transferring) kinase
Glyma.14G001900.1	−1.185	0.0003024	down	NAD-dependent isocitrate dehydrogenase regulatory subunit 1
Glyma.13G144900.1	−2.785	2.46E−08	down	NAD-dependent isocitrate dehydrogenase catalytic subunit 5
Glyma.18G229300.1	−1.612	2.71E−05	down	NAD-dependent malic enzyme
Glyma.09G262900.1	−2.015	4.27E−06	down	NAD-dependent malic enzyme
Glyma.16G059801.1	−1.558	8.43E−06	down	Mitochondrial pyruvate carrier
Glyma.07G128500.1	−1.087	0.0001063	down	Mitochondrial carrier protein CoAc2
Glyma.02G040700.1	−1.229	2.27E−05	down	Mitochondrial dicarboxylate carrier
Glyma.01G024000.1	−1.681	1.81E−05	down	Mitochondrial dicarboxylate carrier

Abbreviations: down, downregulated; FC, fold-change; TCA, tricarboxylic acid; up, upregulated.

Pyruvate dehydrogenase kinases (PDKs; Glyma.09G079000 and Glyma.15G188500), which inhibit the enzymatic conversion of pyruvate to acetyl-CoA by the pyruvate dehydrogenase complex, were significantly upregulated. Meanwhile, a mitochondrial pyruvate carrier (Glyma.16G059801) and a coenzyme A carrier (CoAc2; Glyma.07G128500) were downregulated. The combined result of these changes is expected to reduce acetyl-CoA synthesis in mitochondria, shunting the conventional cyclic TCA cycle (Figure 5). Moreover, isocitrate dehydrogenase catalytic subunit 5 (Glyma.13G144900) and regulatory subunit 1 (Glyma.14G001900) were significantly downregulated in nodule mitochondria, indicating a decreased conversion rate of isocitrate to 2-oxoglutarate (2-OG) (Figure 6).

If acetyl-CoA synthesis is reduced in nodule mitochondria, the cyclic TCA cycle would be slowed down, and an alternative pathway should take place for NADH production (Figure 5). Hence, cytosolic malate would enter the nodule mitochondria and be oxidised via mitochondrial MDH to OAA. Meanwhile, two mitochondrial NAD-dependent ME (Glyma.09G262900 and Glyma.18G229300) were downregulated, suppressing the decarboxylation of malate to pyruvate in nodule mitochondria (Table 1, Figure 6). This means the flux of malate was enhanced toward OAA regeneration instead of pyruvate production. The lowered supply of acetyl-CoA would then limit the conversion of OAA to citrate, promoting OAA accumulation and export. Taken together, the flux of cyclic TCA cycle was systematically downregulated in nodules, and malate oxidation functioned as the primary pathway in carboxylic acid oxidation. Hence, malate oxidation became the major source of NADH for the mitochondrial electron transport chain (mETC) in ATP synthesis in nodules.

Furthermore, two mitochondrial dicarboxylate carriers (DICs; Glyma.01G024000 and Glyma.02G040700) were downregulated in nodule mitochondria. DICs can transport a wide range of dicarboxylates, including malate, OAA, succinate and, less efficiently, 2-OG (Palmieri, Picault, et al., 2008). AtDIC2 was shown to participate in the import of cytosolic malate in exchange for the export of mitochondrial citrate (Lee et al., 2021). In this context, the downregulation of DICs proteins in the nodule may be an adaptation to the reduced production of citrate resulting from the decrease in acetyl-CoA synthesis.

3.3 | Identification of energy state sensors that divert the flux of PEP to OAA in nodules

Among nodule-unique proteins, two cystathionine β-synthase (CBS) domain-containing proteins were identified, namely nodule AMP

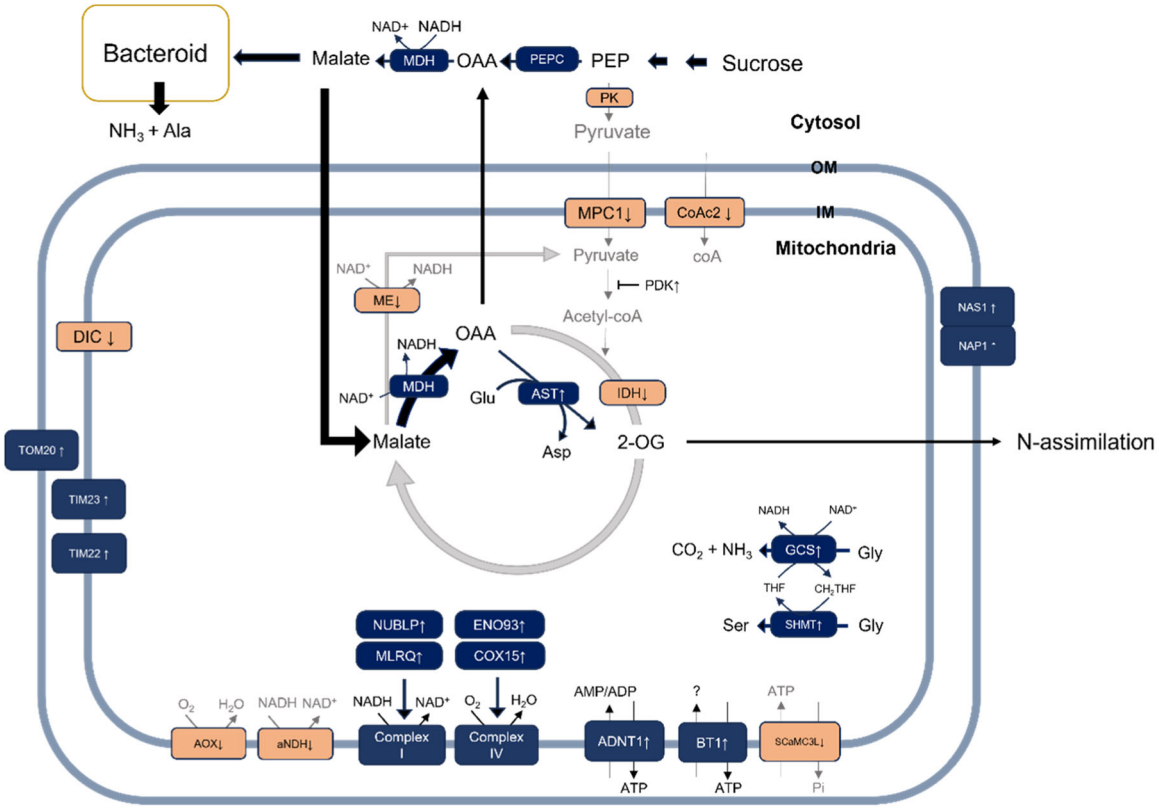

FIGURE 5 Schematic showing proteomic adaptations in the soybean nodule mitochondrion. Differential protein expressions detected in the proteomic data are indicated by up or down arrows (up arrow, upregulated; down arrow, downregulated) alongside the protein name abbreviations. Downregulated and upregulated proteins are also distinguished in orange and blue boxes, respectively. In addition, downregulated pathways are coloured in grey. ADNT1, adenine nucleotide transporter 1; Ala, alanine; AOX, alternative oxidase; aNDH, alternative NAD(P)H-ubiquinone oxidoreductases; Asn, asparagine; AST1, aspartate aminotransferase 1; BT1, Brittle 1; CoA, coenzyme A; CoAc2, CoA carrier 2; COX15, cytochrome c oxidase assembly factor 15; DICs, dicarboxylate carriers; ENO93, early nodulin 93; GCS1, glycine cleavage system 1; Glu, glutamate; IDH, isocitrate dehydrogenase; MDH, malate dehydrogenase; ME, malic enzyme; MLRQ, complex I MLRQ subunit; MPC, mitochondria pyruvate carrier; NAP1, NAS1-associated protein 1; NAS1, nodule AMP sensor 1; NUBPL, nucleotide-binding protein-like; OAA, oxaloacetate; PEP, phosphoenolpyruvate; PEPC, phosphoenolpyruvate carboxylase; PK, pyruvate kinase; SCaMC3L, calcium-binding mitochondrial carrier protein ScaMC-3-like; SHMT, serine hydroxymethyltransferase; TIM22, translocase of inner membrane 22; TIM23, translocase of inner membrane 23; TOM20, translocase of outer membrane 20. [Color figure can be viewed at wileyonlinelibrary.com]

sensor 1 (GmNAS1; Glyma.06G158200) and NAS1-associated protein 1 (GmNAP1; Glyma.04G207600). GmNAS1 and GmNAP1 function as nodule-specific energy sensors involved in the regulation of PEP allocation in the soybean nodule (Ke et al., 2022). Though predicted with peroxisomal localisation by DeepLoc2.0 here, the two CBS proteins were previously shown to be specifically localised to the outer membranes of nodule mitochondria via fluorescence microscopy (Ke et al., 2022). The GmNAS1 and GmNAP1 were demonstrated to form homodimers and bind to a nuclear factor-Y C subunit (GmNFYC10a, Glyma.12g069100), which is a transcription factor that promotes the expression of glycolytic enzymes, including PKs (Ke et al., 2022). Therefore, GmNAS1 and GmNAP1 homodimers likely prevent the nuclear import of GmNFYC10a by maintaining its localisation on mitochondria, thus lowering the downstream expressions of PKs and increasing the flux of PEP toward OAA synthesis in the nodule.

3.4 | Changes in oxidative energy metabolism in the nodule

The assembly factors of the respiratory chain were significantly induced in nodule mitochondria, including NUBPL-like (Glyma.10G034100), COX15-like (Glyma.02G303400.1) and complex I MLRQ subunit (Glyma.08G250300) (Table 2), where these proteins could enhance the cellular respiratory activities of Complexes I and IV. Meanwhile, the expression of AOX (Glyma.08G072200.1) was significantly decreased (Figure 6), as well as alternative NAD(P)H-ubiquinone oxidoreductases (aNDHs; Glyma.12G094000, Glyma.12G094100 and Glyma.12G107000). These changes could reduce the wasteful consumption of electrons by AOX and aNDHs and thus maximise the efficiency of NADH oxidation in the respiratory chain for generating the membrane potential for ATP production (Figure 5).

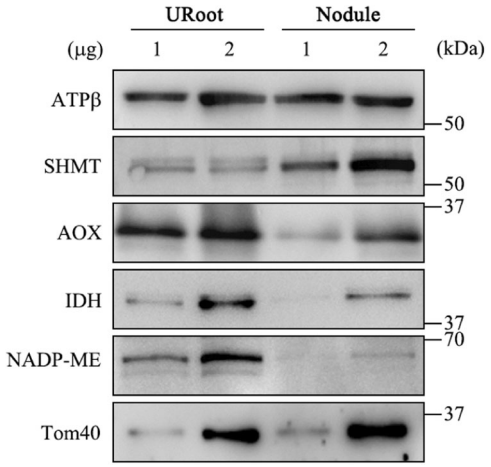

FIGURE 6 Immunoblot validations of soybean mitochondrial proteins extracted from uninoculated roots and nodules. One and 2 μg each of soybean mitochondrial proteins extracted from uninoculated roots (URoot) and nodules (Nodule) were separated by SDS-PAGE and blotted with the indicated antibodies. The proteins used here were from a different batch of extractions from the ones used for proteomics. AOX, alternative oxidase; ATPβ, ATP synthase β subunit; IDH, isocitrate dehydrogenase; NADP-ME, NADP-dependent malic enzyme; SHMT, serine hydroxymethyltransferase; Tom40, translocase of outer membrane 40.

In addition, early nodulin-93 (ENO93, Glyma.06G216500), a nodule-specific protein, was identified exclusively in the nodule mitochondrial proteome (Table 2) (Reddy et al., 1998). A functional study of AtENO93 suggested that ENO93 is a mitochondrial protein associated with complex IV functions and contributes to the positive regulation of ATP synthesis rate (Lee et al., 2023). The Arabidopsis knockout mutant *eno93* exhibited a decreased respiratory rate while the overexpression of *AtENO93* increased the abundance of high-ATP-cost amino acids (Lee et al., 2023). Therefore, the GmENO93 expression in nodule mitochondria may enhance ATP synthesis to support the N-assimilation process.

Several photorespiratory enzymes, including subunits of the glycine cleavage system (GCS1), glycine decarboxylase (Glyma.17G228800) and aminomethyltransferase (Glyma.15G109300), and SHMT (Glyma.18G150000), had significantly higher abundances in the nodule (Table 2, Figure 6). It is possible that nodule mitochondria could also enhance the degradation of glycine to generate additional NADH for cellular respiration.

3.5 | Regulation of adenine nucleotide transport in the nodule

The expression of a mitochondrial adenine nucleotide transporter (ADNT1; Glyma.16G027100) was upregulated while that of a

TABLE 2 Differentially expressed mitochondrial proteins involved in oxidative energy metabolism.

Protein_ID	Log_2FC	Adj. *p*-value	Differential expression	Protein description
Glyma.06G216500.1	NA	NA	Nodule-unique	Early nodulin-93
Glyma.12G094000.2	NA	NA	Root-unique	Apoptosis-inducing factor homologue A-like isoform X2
Glyma.12G094100.1	NA	NA	Root-unique	Uncharacterised protein LOC100813980
Glyma.08G250300.1	6.620	9.67E−09	up	NADH-ubiquinone reductase Complex 1 MLRQ Subunit
Glyma.17G228800.1	1.670	5.98E−05	up	Mitochondrial glycine dehydrogenase (decarboxylating)
Glyma.10G034100.1	1.596	2.34E−06	up	Iron-sulphur protein NUBPL-like isoform X1
Glyma.15G109300.1	1.569	9.37E−06	up	Aminomethyltransferase, mitochondrial-like
Glyma.18G150000.1	1.469	1.72E−05	up	Serine hydroxymethyltransferase 5
Glyma.02G303400.1	1.420	2.57E−05	up	Cytochrome c oxidase assembly protein COX15-like
Glyma.12G107000.1	−2.065	1.46E−07	down	External alternative NAD(P)H-ubiquinone oxidoreductase B1
Glyma.08G072200.1	−1.187	3.79E−05	down	Alternative oxidase 3, mitochondrial [*Glycine max*]

Abbreviations: down, downregulated; FC, fold-change; up, upregulated.

TABLE 3 Differentially expressed mitochondrial proteins involved in adenine nucleotide transport in nodules.

Protein_ID	Log_2FC	Adj. *p*-value	Differential expression	Protein description
Glyma.16G027100.1	1.296	6.39E−04	up	Mitochondrial adenine nucleotide transporter ADNT1
Glyma.19G105600.1	−1.204	6.35E−05	down	Calcium-binding mitochondrial carrier protein SCaMC-3-like
Glyma.06G069500.1	5.698	2.43E−09	up	Adenine nucleotide transporter BT1, chloroplastic/mitochondrial-like
Glyma.04G067800.1	5.277	1.52E−09	up	Adenine nucleotide transporter BT1, chloroplastic/mitochondrial-like
Glyma.17G209500.1	3.501	1.16E−06	up	Adenine nucleotide transporter BT1, chloroplastic/mitochondrial

Abbreviations: down, downregulated; FC, fold-change; up, upregulated.

mitochondrial $MgATP^{2-}$/Pi carrier (SCaMC-3-like; Glyma.19G105600), was downregulated in the nodule mitochondria (Table 3). Functional analyses demonstrated that AtADNT1 mediates the exchange of ATP and AMP between mitochondria and the cytosol (Palmieri, Santoro, et al., 2008). Meanwhile, SCaMC-3-like functions as a calcium-independent $MgATP^{2-}$/Pi exchanger that imports $MgATP^{2-}$ from the cytosol into mitochondria (Traba et al., 2009). Coordinating with the upregulated respiratory chain, ATP transporter expressions in nodule mitochondria were also altered to enhance ATP export from nodule mitochondria.

The protein abundances of three adenine nucleotide transporters, Brittle 1 (BT1; Glyma.04G067800, Glyma.06G069500 and Glyma.17G209500.1), were observed to be significantly increased in nodule mitochondria by more than 10 folds according to the DIA data (Table 3). Interestingly, although they were categorised as members of the mitochondrial carrier family, fluorescence microscopy analyses of the fusion proteins of AtBT1 (from Arabidopsis) and ZmBT1 (from corn) revealed that BT1 proteins are localised in both mitochondria and plastids (Bahaji et al., 2011). In addition, BT1 homologues may have different substrate specificities depending on plant species. The ZmBT1 can mediate the bidirectional ADPglucose/ADP exchange in plastids, but AtBT1 and StBT1 (from potato) can only perform the unidirectional export of AMP, ADP and ATP from plastids (Bahaji et al., 2011; Kirchberger et al., 2008; Leroch et al., 2005). It is likely that soybean BT1s in nodule mitochondria participate in the ATP export to the cytosol.

3.6 | Enhanced expression of the protein import machinery in nodule mitochondria

The majority of mitochondrial proteins originate from nuclear-encoded precursors and have to be imported into mitochondria via a network of protein translocases (Murcha et al., 2014; Song et al., 2021). In nodules, the abundances of the translocase of outer membrane 20 (TOM20; Glyma.11G250100), translocases of inner membrane 23 and 22 (TIM23; Glyma.10G161100 and Glyma.20G223900; and TIM22; Glyma.04G225600 and Glyma.06G139200) were significantly increased (Table 4). TOM20 is a mitochondrial import receptor that recognises mitochondrion-targeting sequences on precursor proteins (Rimmer et al., 2011). Localised in the mitochondrial inner membrane, TIM23 and TIM22 are responsible for the import of various mitochondrial proteins. Matrix-located precursor proteins are imported via the TIM23 complex, whereas mitochondrial carrier proteins are imported via the TIM22 complex for integration into the inner membrane (Bauer et al., 2000). The upregulation of TIM23 and TIM22 abundances likely helps reshape the nodule mitochondrial proteome. For instance, TIM23-overexpression in *Arabidopsis* was associated with an increased rate of protein import (Wang et al., 2012). Also, the import of mitochondrial carrier proteins such as the ATP/ADP carrier is mediated by the TIM22 complex (Bauer et al., 2000; Endres, 1999). In addition, the upregulation of translocases could be responsible for remodelling the respiratory chain, as interactions between translocases and respiratory chain complexes have been found in both plant and nonplant models (Cogliati et al., 2018; Kulawiak et al., 2013; Murcha et al., 2012).

3.7 | Nodule mitochondria synthesise the C-skeleton for symbiotic N-assimilation

Two mitochondrial aspartate aminotransferases (ASTs; Glyma.01G131100 and Glyma.06G275700), were identified in the mitochondrial proteomic data (Supporting Information: Table S1). While Glyma.06G275700 showed no difference in expression levels between nodule and root samples, Glyma.01G131100 was exclusively expressed in nodule mitochondria (Table 5). ASTs are

TABLE 4 Differentially expressed mitochondrial proteins involved in the mitochondrial protein import machinery.

Protein_ID	Log_2FC	Adj. *p*-value	Differential expression	Protein description
Glyma.04G225600.1	1.449	1.53E−05	up	Mitochondrial import inner membrane translocase TIM22
Glyma.06G139200.1	1.693	1.38E−05	up	Mitochondrial import inner membrane translocase TIM22
Glyma.10G161100.1	1.214	8.72E−04	up	Mitochondrial import inner membrane translocase TIM23-1
Glyma.11G250100.1	1.530	3.29E−06	up	Mitochondrial import receptor TOM20
Glyma.20G223900.1	1.575	5.10E−05	up	Mitochondrial import inner membrane translocase TIM23-3

Abbreviations: FC, fold-change; up, upregulated.

TABLE 5 Differentially expressed mitochondrial proteins involved in the conversion of dicarboxylates.

Protein_ID	Log_2FC	Adj. *p*-value	Differential expression	Protein description
Glyma.16G013900.1	0.676	8.83E−03	ns	Alanine aminotransferase 2-like
Glyma.01G131100.1	NA	NA	Nodule-unique	Aspartate aminotransferase, mitochondrial-like
Glyma.02G072200.1	NA	NA	Root-unique	Glutamate dehydrogenase B isoform X2

Abbreviations: FC, fold-change; ns, not significant.

transaminases catalysing the reversible conversion of glutamate and OAA into aspartate and 2-OG. When the mitochondrial OAA level built up, it would be converted into 2-OG by AST. Since the CoAc2 was downregulated in nodules (Table 5), the reduction in coenzyme A import would slow down the conversion of 2-OG into succinyl CoA. Consequently, the excess 2-OG and aspartate would be exported from nodule mitochondria.

Other mitochondrial enzymes involved in amino acid metabolism were differentially expressed in the nodule (Table 5). These include mitochondrial alanine aminotransferase (ALT; Glyma.16G013900), which catalyses the reversible conversion of 2-OG and alanine into pyruvate and glutamate. Though the FC did not meet the threshold of >2, the elevated expression of ALT in nodule mitochondria was nonetheless highly significant (FC = 1.597, adj. *p*-value = $8.83e^{-3}$). Since pyruvate availability is limited in the nodule, it is possible that nodule mitochondrial ALT can partially metabolise alanine, by transferring the amino group from alanine to 2-OG to form glutamate. The pyruvate thus produced could then be metabolised in the downsized TCA cycle in nodule mitochondria. Three glutamate dehydrogenases (GDHs; Glyma.02G072200, Glyma.16G041200 and Glyma.19G111000) were detected with confidence (five out of five replicates) in this experiment (Supporting Information: Table S1). No significant difference was observed for Glyma.16G041200 and Glyma.19G111000 between nodule and root samples. However, Glyma.02G072200 was only detectable in uninoculated roots, meaning a suppressed expression in nodule (Table 5, Supporting Information: Tables S3 and S4).

4 | DISCUSSION

Managing the energy state in symbiotic nodules allows legume plants to optimise carbon utilisation for nitrogen assimilation. To sustain the energy demand in the symbiotic relationship, nodulation requires whole-system adjustments in carbon and nitrogen metabolism. Using the quantitative DIA strategy, we highlighted the proteomic differences between the mitochondria isolated from nodules and uninoculated roots. In conventional bottom-up proteomic, DDA serves as a reliable and straight-forward method of choice for peptide identification. However, DDA based quantitative proteomic often presents the quantitative challenges of missing values, high abundance bias and low reproducibility, originated from the stochastic peptide sampling based on MS1 survey scan (Dowell et al., 2021; Ting et al., 2015). In contrast to DDA mode, DIA-based analysis cycles through wide *m/z* windows in which all peptide ions within the isolation windows are subjected to fragmentation in an unbiased manner. Such unbiased peptide sampling in DIA thus allows less missing values, wider proteome coverage and higher quantitative accuracy (Dowell et al., 2021; Kitata et al., 2023; Krasny & Huang, 2021). Combining the strengths of DDA-based spectral library and DIA-based quantification, the quantitative proteomic data in this study provides a comprehensive overview of the proteomic adaptations in energy production and carbon utilisation in soybean nodule mitochondria.

Modulating metabolic pathways in carbon allocation is crucial in nodule symbiosis. At the epigenetic level, many genes involved in

carbon and nitrogen metabolism in soybean nodules are systematically modified with the H3K4me3 histone mark, with most of the genes in the sucrose metabolic and glycolytic pathways being highly expressed due to elevated H3K4me3 (Wang et al., 2020). The transcriptions of *PEPC* and *MDH* have been reported to be upregulated in nodules, explaining the flux of PEP toward the synthesis of malate instead of pyruvate (Miller et al., 1998; Nakagawa et al., 2003; Wang et al., 2020). In fact, at optimal pH, the maximal PEPC capacity is 2.6X of PK in crude nodule extract (McCloud et al., 2001). Under normal growth condition, the levels of OAA (~330 nmol g^{-1} fresh weight [FW]) and malate (~3500 nmol g^{-1} FW) in 25 DPI soybean nodules are much higher than that of pyruvate (~180 nmol g^{-1} FW). Extra supply of sucrose increased the levels of OAA (12.1X to ~4000 nmol g^{-1} FW) and malate (2.3X to ~8000 nmol g^{-1} FW) in nodules, whereas the level of pyruvate remained constant (~180 nmol g^{-1} FW) (Ke et al., 2022). These data corroborated with our proteomics data and supported the notion that in nodules the majority of source sucrose is converted into OAA via the action of PEPC and then to malate via the action of cytosolic MDH. Thermodynamically, the reversible reaction catalysed by MDH greatly favours the production of malate and as a result OAA is not always detectable in metabolomics studies (Sun et al., 2012). The high OAA concentration in soybean nodule is surprising, indicating a strong flux of PEP to OAA via PEPC and a high flux of malate oxidation in mitochondria which regenerates OAA. As a compensation for the reduction in the PEP flux towards pyruvate production, a portion of the cytosolic malate enters the nodule mitochondrion as a source of NADH for energy production by the mETC. As shown in our proteomic data, there were significant changes in the protein abundances of the mitochondrial enzymes involved in malate and pyruvate metabolism in general, indicating a modification of the TCA cycle flux (Figure 5). However, inconsistent with transcriptomic data in soybean nodule (Wang et al., 2020), no statistically significant difference could be observed with the mitochondrial MDH abundance in nodules. This may be due to the mitochondrion having a high level of MDH to begin with, and so the flux of malate-to-OAA conversion was likely limited by malate and NAD^+ availability rather than the amount of enzyme. Still, in the nodule mitochondrial proteome, the expressions of pyruvate carriers and coA carriers were downregulated, while those of PDKs were upregulated, and NAD-dependent MEs were downregulated (Table 1, Figure 6). The results strongly suggested the conversion of malate into OAA proceeded via MDH rather than other enzymatic steps in the cyclic TCA cycle, was the primary pathway for NADH production in nodule mitochondria. The downregulation of pyruvate metabolism in nodule mitochondria also helped to reduce the flux through the regular TCA cycle for the conversion of OAA into citrate acid. This could thus preserve OAA for malate regeneration in the plastid and cytosol. Our proteomic data thus were in line with the metabolome (Ke et al., 2022) and the enzymatic activity assays on soybean and cowpea nodules (Bryce & Day, 1990; McCloud et al., 2001; Rawsthorne & Larue, 1986).

In vitro experiments on soybean nodules suggested that after malate is converted into OAA, the OAA is rapidly exported from mitochondria (Booth et al., 2021; Bryce & Day, 1990). Nevertheless, one mitochondrial AST (Glyma.01G131100) was found exclusively expressed in nodules in our data set (Table 5). The upregulation of *Glyma.01G131100* was also observed in the transcriptomic data from soybean nodules (Wang et al., 2020). These findings suggest that mitochondrial OAA could be further metabolised into 2-OG by transamination with glutamate via the AST activity, which were also detected in isolated mitochondria from soybean nodule (Bryce & Day, 1990). The resulting 2-OG and aspartate can then be transported out of mitochondria for N-assimilation. 2-OG can enter the GS/GOGAT system for N-assimilation via the synthesis of glutamate and glutamine. Meanwhile, exported aspartate can contribute to N-assimilation pathways via asparagine synthetase that catalyses the amidation of aspartate using glutamine or, at a lower affinity, ammonium ions as substrates (Gaufichon et al., 2010; Huber & Streeter, 1985).

Soybean or pea nodule bacteroids were reported to excrete mixtures of ammonium ions and amino acids, such as alanine and aspartate, to host cells (Rosendahl et al., 1992; Schulte et al., 2021; Waters et al., 1998). Analyses on *ex planta* soybean bacteroids demonstrated that the shift toward the mixed excretion of ammonium ions and amino acids (predominantly alanine) was directly proportional to the bacteroid density, partial pressure of oxygen, and malate content (Waters et al., 2020). Therefore, it is possible that the alanine excreted from bacteroids enters the root cell cytosol as an alternative nitrogen source. This phenomenon may explain the differential expression of enzymes involved in amino acid metabolism in the host nodule. In soybean nodules, both the transcript levels and enzymatic activities of mitochondrial ALTs were shown to be upregulated, compared to those in uninoculated roots, and the total alanine content in the nodule was also higher than in the uninoculated root (Rocha et al., 2010). An upregulation of the mitochondrial ALT expression in nodule cells was also observed in the proteomic data from *Vicia faba* (broad bean) (Thal et al., 2018). As bacteroids export ammonia and alanine to the host plant, it is possible that alanine is partially assimilated in mitochondria by ALT. The upregulation of nodule mitochondrial ALT may enable alanine supplied by bacteroids to be partially metabolised and allow the conversion of 2-OG into glutamate via transamination.

GDHs were once considered to be involved in N-assimilation, owing to their ability to reversibly convert 2-OG to glutamate, but functional studies of the enzymes suggested that GDHs mainly catalyse the deamination of glutamate (Dubois et al., 2003). In our proteomic results, the protein expression of one GDH (Glyma.02G072200) was found suppressed in nodule mitochondria, though the other two GDHs were not differentially expressed (Table 5). Similarly, the expression of GDH transcripts were reported to be downregulated in the nodules of alfalfa and *Virgilia divaricata* (Magadlela et al., 2019; Trepp, Temple, et al., 1999). The reduction in nodule mitochondrial GDH expressions may enhance the efficiency of N-assimilation, as it minimises glutamate consumption in mitochondria.

Since the TCA cycle is slowed down in the soybean nodule mitochondria, one would expect a lower rate of succinate synthesis. Furthermore, soybean and chickpea nodules were shown to contain a larger quantity of malonate, which is an inhibitor of mitochondrial succinate dehydrogenase (Kim & Kim, 1999; Li & Copeland, 2000; Streeter, 1987). We therefore reasoned that the contribution of complex II to nodule respiration would be limited due to a lower amount of succinate as substrate and the inhibitory effect from malonate. To maintain the required level of ATP synthesis, nodule mitochondria would have to compensate by increasing the activities of the other NADH-oxidising complexes in the respiratory chain. We found that the regulatory factors responsible for the complexes I and IV of the electron transport chain were upregulated in nodule mitochondria (Table 2), which could make up for the shortfall in ATP synthesis due to a reduction in the Complex II function. Alternative NDHs, which dissipate excess electrons fed into the mETC by the NADH-oxidising activity of complex I, were downregulated in nodule mitochondria. Likewise, AOX, a nonproton pumping oxidase that bypasses complexes III and IV, was also downregulated, thus reducing its competition for oxygen with complex IV in the nodule (Vanlerberghe, 2013) (Figure 6). On the other hand, photorespiratory enzymes which generate NADH via glycine degradation were induced in the nodule.

Furthermore, beyond proteome remodelling, host plants could accommodate symbiotic nitrogen fixation by rearranging the distribution of organelles in nodule cells. In soybean nodules, mitochondria are concentrated on the periphery of the infected cells. In particular, nodule mitochondria are localised next to the gas-filled intercellular space, which is predicted to have a higher oxygen concentration (Millar et al., 1995). Moreover, it was demonstrated that soybean nodules can maintain a higher respiration rate in low oxygen concentration than in uninoculated roots, suggesting a relatively higher oxygen affinity in cytochrome pathway in nodule mitochondria (Millar et al., 1995). Knowledge of the nodule anatomy thus offers a key context for understanding the proteomic data. Through the positioning of nodule mitochondria near the gas-filled intercellular space and the upregulation of complex IV activities, host cells could maintain the respiratory rate despite the microaerobic condition in the infected zone (Thumfort et al., 1999). Together with the modulated complex I function, the remodelling of respiratory chain could thus keep up with ATP synthesis for nodule metabolism.

Meanwhile, the intracellular distribution of plastids is closely associated with mitochondria around the periphery in soybean nodule cells (Millar et al., 1995). This close association can be biologically significant in facilitating the coordinated N-assimilation metabolism between organelles, and it may also explain the relatively high degree of plastidic contamination in nodule mitochondrial protein extracts. Nodule plastids play a significant role in the regeneration of NADPH via the partial metabolism of shoot-derived sucrose by the OPPP to provide the reducing power necessary for N-assimilation (Hong & Copeland, 1990; Kohl et al., 1990; Lepetit & Brouquisse, 2023). The OPPP activity may also be crucial in maintaining the cellular redox balance by regulating the NADPH concentration under the microaerobic condition in the nodule (Ralser et al., 2007). Moreover, plastidic OPPP provides an alternate route of carbon allocation for N-assimilation by generating R5P. In the nodule plastids, R5P can subsequently serve as the precursor for the de novo purine biosynthesis pathway, which feeds into ureide production (Liu et al., 2018; Smith & Atkins, 2002; Tajima, 2004). Plastids are also responsible for housing key enzymes involved in N-assimilation, including the plastidic isoforms of AST, GS and GOGAT (Lea & Miflin, 2003; De La Torre et al., 2014; Trepp, Plank, et al., 1999; Valderrama-Martín et al., 2022). For instance, a study of *L. japonicus* mutants deficient in plastidic GS reported that in the mutant nodule, there was up to 40% loss of total GS activity compared to wild type (García-Calderón et al., 2012). Therefore, nodule plastids significantly contribute to the process of nitrogen fixation. The close contact between mitochondria and plastids not only facilitates the exchange of metabolites essential for N-assimilation, including the transport of 2-OG and glutamate which are central to the N-assimilation pathway, but it also allows the rapid exchange of adenosine nucleotides to meet the ATP demand for GS/GOGAT and purine biosynthesis, as reflected by the upregulation of ATP transporters on mitochondrial membranes that favours ATP export.

The modulation of energy metabolism in nodules can be dynamic according to the physiological state. We identified the CBS-domain proteins, GmNAS1 and GmNAP1, as specifically expressed in the nodule. GmNAS1 and GmNAP1 are responsible for the regulation of PEP allocation that determines the carbon flux in the nodule, by preventing the entry of the transcription factor GmNFYC10a, an activator of glycolytic enzyme genes including PKs, into the nucleus (Ke et al., 2022). Under normal growth condition, GmNAS1 and GmNAP1 can form homodimers and interact with GmNFYC10a on the mitochondrial membrane, preventing its entry into the nodule nucleus. By preventing the nuclear localisation of GmNFYC10a, GmNAS1 and GmNAP1 can inhibit pyruvate synthesis, therefore favoring the use of PEP for OAA synthesis instead. Conversely, in the low energy state (e.g., in root hair where the sucrose supply is lower), AMP binding to GmNAS1can disrupt the GmNAS1-GmNFYC10a interaction, promoting the nuclear localisation of GmNFYC10a and activating pyruvate synthesis for energy production (Ke et al., 2022).

The possible existence of an energy-sensing flux model driven by CBS proteins is one example that showcases the plasticity of nodule metabolism. Based on the data from this study, we proposed a probable nodule-specific energy-sensing carbon flux switching model. Under normal growth condition with amply sucrose supply, the nodule is optimised for N-assimilation and malate production. PK expression is reduced and PEPC expression is increased, promoting the conversion of PEP to malate to facilitate nitrogen fixation in bacteroids. Since pyruvate metabolism is suppressed, oxidation of malate to OAA by mitochondrial MDH becomes a primary source of energy, and OAA can be either exported or metabolised into 2-OG (Figure 5). Under low sucrose supply, the nodules revert to normal energy metabolism, utilising pyruvate and the conventional cyclic TCA cycle to synthesise ATP for the basic cellular activities, while sacrificing the nitrogen fixation in bacteroids.

5 | CONCLUSION

In conclusion, soybean nodule cells reshape the energy metabolic pathways to increase malate supply to rhizobia, by modulating the nodule mitochondrial proteome and metabolism. There is now consensus that PEP is preferably converted to OAA instead of pyruvate in nodules. This offers two advantages. First, root cells do not have Rubisco to fix CO_2 and therefore the conversion of PEP to OAA is a mean of fixing CO_2. The enhanced PEP flux to OAA has an additional advantage over the flux to pyruvate. In nodule, both the bacteroides and root cells respirated intensively and release a high flux of CO_2. The PEPC reaction can fix CO_2 respirated by the nodule mitochondria and bacteroids and convert a C3 compound into a C4 compound. The use of NADH generated from malate instead of pyruvate can also reduce CO_2 release from the TCA cycle. Second, this pathway enhances malate synthesis, which serves as the major carbon source to feed rhizobia and support symbiosis and nitrogen fixation in nodules. Hence, there are physiological advantages for nodule root cells to prefer PEPC pathway and the use of malate as the fuel for mitochondria. Through quantitative proteomic comparisons, we showed that soybean nodule mitochondria operate under a modulated TCA cycle that utilises malate as the source of NADH synthesis, and OAA is converted to 2-OG to form the C-skeleton for N-assimilation. To enhance the capacity of ATP synthesis required for nodule symbiosis and energy-intensive nitrogen fixation, extensive modulations were observed in the mitochondrial respiratory chain and adenylate transporters. The proteomic results presented here not only confirmed the findings of past studies but also provided novel detailed understanding of the energy metabolism in nodules.

ACKNOWLEDGEMENTS

This work was supported by the Hong Kong Research Grants Council Area of Excellence Scheme (AoE/M-403/16), and the Innovation and Technology Fund (Funding Support to State Key Laboratory of Agrobiotechnology) from the Hong Kong Special Administrative Region, China. Any opinions, findings, conclusions or recommendations expressed in this publication do not reflect the view of the Government of the Hong Kong Special Administrative Region or the Innovation and Technology Commission.

CONFLICT OF INTEREST STATEMENT

The authors declare no conflict of interest.

DATA AVAILABILITY STATEMENT

The data that support the findings of this study are openly available in ProteomeXchange Consortium at https://www.proteomexchange.org/, reference number PXD050301.

ORCID

Wai-Ching Sin http://orcid.org/0000-0003-0783-1707
Hon-Ming Lam http://orcid.org/0000-0002-6673-8740
Boon Leong Lim http://orcid.org/0000-0002-2720-2353

REFERENCES

Almagro Armenteros, J.J., Salvatore, M., Emanuelsson, O., Winther, O., Von Heijne, G., Elofsson, A. et al. (2019) Detecting sequence signals in targeting peptides using deep learning. *Life Science Alliance*, 2, e201900429. Available from: https://doi.org/10.26508/lsa.201900429.

Bahaji, A., Ovecka, M., Bárány, I., Risueño, M.C., Muñoz, F.J., Baroja-Fernández, E. et al. (2011) Dual targeting to mitochondria and plastids of AtBT1 and ZmBT1, two members of the mitochondrial carrier family. *Plant and Cell Physiology*, 52, 597–609. Available from: https://doi.org/10.1093/pcp/pcr019

Bauer, M.F., Hofmann, S., Neupert, W. & Brunner, M. (2000) Protein translocation into mitochondria: the role of TIM complexes. *Trends in Cell Biology*, 10, 25–31. Available from: https://doi.org/10.1016/S0962-8924(99)01684-0

Booth, N.J., Smith, P.M.C., Ramesh, S.A. & Day, D.A. (2021) Malate transport and metabolism in nitrogen-fixing legume nodules. *Molecules*, 26, 6876. Available from: https://doi.org/10.3390/molecules26226876

Bryce, J.H. & Day, D.A. (1990) Tricarboxylic acid cycle activity in mitochondria from soybean nodules and cotyledons. *Journal of Experimental Botany*, 41, 961–967. Available from: https://doi.org/10.1093/jxb/41.8.961

Carrie, C. & Small, I. (2013) A reevaluation of dual-targeting of proteins to mitochondria and chloroplasts. *Biochimica et Biophysica Acta (BBA) – Molecular Cell Research*, 1833, 253–259. Available from: https://doi.org/10.1016/j.bbamcr.2012.05.029

Cogliati, S., Lorenzi, I., Rigoni, G., Caicci, F. & Soriano, M.E. (2018) Regulation of mitochondrial electron transport chain assembly. *Journal of Molecular Biology*, 430, 4849–4873. Available from: https://doi.org/10.1016/j.jmb.2018.09.016

Dam, S., Dyrlund, T.F., Ussatjuk, A., Jochimsen, B., Nielsen, K., Goffard, N. et al. (2014) Proteome reference maps of the *Lotus japonicus* nodule and root. *Proteomics*, 14, 230–240. Available from: https://doi.org/10.1002/pmic.201300353

Day, D., Neuburger, M. & Douce, R. (1985) Biochemical characterization of chlorophyll-free mitochondria from pea leaves. *Functional Plant Biology*, 12, 219. Available from: https://doi.org/10.1071/PP9850219

Deutsch, E.W., Bandeira, N., Perez-Riverol, Y., Sharma, V., Carver, J.J., Mendoza, L. et al. (2023) The ProteomeXchange consortium at 10 years: 2023 update. *Nucleic Acids Research*, 51, D1539–D1548. Available from: https://doi.org/10.1093/nar/gkac1040

Dowell, J.A., Wright, L.J., Armstrong, E.A. & Denu, J.M. (2021) Benchmarking quantitative performance in label-free proteomics. *ACS Omega*, 6, 2494–2504. Available from: https://doi.org/10.1021/acsomega.0c04030

Dubois, F., Tercé-Laforgue, T., Gonzalez-Moro, M.-B., Estavillo, J.-M., Sangwan, R., Gallais, A. et al. (2003) Glutamate dehydrogenase in plants: is there a new story for an old enzyme? *Plant Physiology and Biochemistry*, 41, 565–576. Available from: https://doi.org/10.1016/S0981-9428(03)00075-5

Duncan, O., Taylor, N.L., Carrie, C., Eubel, H., Kubiszewski-Jakubiak, S., Zhang, B. et al. (2011) Multiple lines of evidence localize signaling, morphology, and lipid biosynthesis machinery to the mitochondrial outer membrane of Arabidopsis. *Plant Physiology*, 157, 1093–1113. Available from: https://doi.org/10.1104/pp.111.183160

Endres, M. (1999) Transport of the ADP/ATP carrier of mitochondria from the TOM complex to the TIM2254 complex. *The EMBO Journal*, 18, 3214–3221. Available from: https://doi.org/10.1093/emboj/18.12.3214

Fedorova, M., Tikhonovich, I.A. & Vance, C.P. (1999) Expression of C-assimilating enzymes in pea (*Pisum sativum* L.) root nodules. *In situ* localization in effective nodules. *Plant, Cell & Environment*, 22,

1249–1262. Available from: https://doi.org/10.1046/j.1365-3040.1999.00490.x

García-Calderón, M., Chiurazzi, M., Espuny, M.R. & Márquez, A.J. (2012) Photorespiratory metabolism and nodule function: behavior of *Lotus japonicus* mutants deficient in plastid glutamine synthetase. *Molecular Plant–Microbe Interactions®*, 25, 211–219. Available from: https://doi.org/10.1094/MPMI-07-11-0200

Gaufichon, L., Reisdorf-Cren, M., Rothstein, S.J., Chardon, F. & Suzuki, A. (2010) Biological functions of asparagine synthetase in plants. *Plant Science*, 179, 141–153. Available from: https://doi.org/10.1016/j.plantsci.2010.04.010

Hong, Z.Q. & Copeland, L. (1990) Pentose phosphate pathway enzymes in nitrogen-fixing leguminous root nodules. *Phytochemistry*, 29, 2437–2440. Available from: https://doi.org/10.1016/0031-9422(90)85162-9

Huber, T.A. & Streeter, J.G. (1985) Purification and properties of asparagine synthetase from soybean root nodules. *Plant Science*, 42, 9–17. Available from: https://doi.org/10.1016/0168-9452(85)90022-6

Ke, X., Xiao, H., Peng, Y., Wang, J., Lv, Q. & Wang, X. (2022) Phosphoenolpyruvate reallocation links nitrogen fixation rates to root nodule energy state. *Science*, 378, 971–977. Available from: https://doi.org/10.1126/science.abq8591

Kim, H.-M. & Kim, Y.S. (1999) Identification of malonate derivates from legume nodules: possible evidence of the malonate shuttle from soybean and clover nodules. *Journal of Plant Physiology*, 155, 126–128. Available from: https://doi.org/10.1016/S0176-1617(99)80152-7

Kirchberger, S., Tjaden, J. & Ekkehard Neuhaus, H. (2008) Characterization of the Arabidopsis Brittle1 transport protein and impact of reduced activity on plant metabolism. *The Plant Journal*, 56, 51–63. Available from: https://doi.org/10.1111/j.1365-313X.2008.03583.x

Kisslov, I., Naamati, A., Shakarchy, N. & Pines, O. (2014) Dual-targeted proteins tend to be more evolutionarily conserved. *Molecular Biology and Evolution*, 31, 2770–2779. Available from: https://doi.org/10.1093/molbev/msu221

Kitata, R.B., Yang, J.C. & Chen, Y.J. (2023) Advances in data-independent acquisition mass spectrometry towards comprehensive digital proteome landscape. *Mass Spectrometry Reviews*, 42, 2324–2348. Available from: https://doi.org/10.1002/mas.21781

Kohl, D.H., Lin, J.-J., Shearer, G. & Schubert, K.R. (1990) Activities of the pentose phosphate pathway and enzymes of proline metabolism in legume root nodules. *Plant Physiology*, 94, 1258–1264. Available from: https://doi.org/10.1104/pp.94.3.1258

Krasny, L. & Huang, P.H. (2021) Data-independent acquisition mass spectrometry (DIA-MS) for proteomic applications in oncology. *Molecular Omics*, 17, 29–42. Available from: https://doi.org/10.1039/D0MO00072H

Kulawiak, B., Höpker, J., Gebert, M., Guiard, B., Wiedemann, N. & Gebert, N. (2013) The mitochondrial protein import machinery has multiple connections to the respiratory chain. *Biochimica et Biophysica Acta (BBA) – Bioenergetics*, 1827, 612–626. Available from: https://doi.org/10.1016/j.bbabio.2012.12.004

Lea, P.J. & Miflin, B.J. (2003) Glutamate synthase and the synthesis of glutamate in plants. *Plant Physiology and Biochemistry*, 41, 555–564. Available from: https://doi.org/10.1016/S0981-9428(03)00060-3

Lee, C.P., Elsässer, M., Fuchs, P., Fenske, R., Schwarzländer, M. & Millar, A.H. (2021) The versatility of plant organic acid metabolism in leaves is underpinned by mitochondrial malate–citrate exchange. *The Plant Cell*, 33, 3700–3720. Available from: https://doi.org/10.1093/plcell/koab223

Lee, C.P., Le, X.H., Gawryluk, R.M.R., Casaretto, J.A., Rothstein, S.J. & Millar, A.H. (2023) ENOD93 interacts with cytochrome c oxidase altering respiratory ATP production and root growth in plants (preprint). *bioRvix*. Available from: https://doi.org/10.1101/2023.04.15.535782

Lepetit, M. & Brouquisse, R. (2023) Control of the rhizobium–legume symbiosis by the plant nitrogen demand is tightly integrated at the whole plant level and requires inter-organ systemic signaling. *Frontiers in Plant Science*, 14, 1114840. Available from: https://doi.org/10.3389/fpls.2023.1114840

Leroch, M., Kirchberger, S., Haferkamp, I., Wahl, M., Neuhaus, H.E. & Tjaden, J. (2005) Identification and characterization of a novel plastidic adenine nucleotide uniporter from *Solanum tuberosum*. *Journal of Biological Chemistry*, 280, 17992–18000. Available from: https://doi.org/10.1074/jbc.M412462200

Li, J. & Copeland, L. (2000) Role of malonate in chickpeas. *Phytochemistry*, 54, 585–589. Available from: https://doi.org/10.1016/S0031-9422(00)00162-X

Liu, A., Contador, C.A., Fan, K. & Lam, H.-M. (2018) Interaction and regulation of carbon, nitrogen, and phosphorus metabolisms in root nodules of legumes. *Frontiers in Plant Science*, 9, 1860. Available from: https://doi.org/10.3389/fpls.2018.01860

Magadlela, A., Morcillo, R.J.L., Kleinert, A., Venter, M., Steenkamp, E. & Valentine, A. (2019) Glutamate dehydrogenase is essential in the acclimation of *Virgilia divaricata*, a legume indigenous to the nutrient-poor Mediterranean-type ecosystems of the Cape Fynbos. *Journal of Plant Physiology*, 243, 153053. Available from: https://doi.org/10.1016/j.jplph.2019.153053

Matamoros, M.A., Fernández-García, N., Wienkoop, S., Loscos, J., Saiz, A. & Becana, M. (2013) Mitochondria are an early target of oxidative modifications in senescing legume nodules. *New Phytologist*, 197, 873–885. Available from: https://doi.org/10.1111/nph.12049

McCloud, S.A., Smith, R.G. & Schuller, K.A. (2001) Partial purification and characterization of pyruvate kinase from the plant fraction of soybean root nodules. *Physiologia Plantarum*, 111, 283–290. Available from: https://doi.org/10.1034/j.1399-3054.2001.1110304.x

Millar, A.H., Day, D.A. & Bergersen, F.J. (1995) Microaerobic respiration and oxidative phosphorylation by soybean nodule mitochondria: implications for nitrogen fixation. *Plant, Cell & Environment*, 18, 715–726. Available from: https://doi.org/10.1111/j.1365-3040.1995.tb00574.x

Miller, S.S., Driscoll, B.T., Gregerson, R.G., Gantt, J.S. & Vance, C.P. (1998) Alfalfa malate dehydrogenase (MDH): molecular cloning and characterization of five different forms reveals a unique nodule-enhanced MDH. *The Plant Journal*, 15, 173–184. Available from: https://doi.org/10.1046/j.1365-313X.1998.00192.x

Murcha, M.W., Kmiec, B., Kubiszewski-Jakubiak, S., Teixeira, P.F., Glaser, E. & Whelan, J. (2014) Protein import into plant mitochondria: signals, machinery, processing, and regulation. *Journal of Experimental Botany*, 65, 6301–6335. Available from: https://doi.org/10.1093/jxb/eru399

Murcha, M.W., Wang, Y. & Whelan, J. (2012) A molecular link between mitochondrial preprotein transporters and respiratory chain complexes. *Plant Signaling & Behavior*, 7, 1594–1597. Available from: https://doi.org/10.4161/psb.22250

Nakagawa, T., Izumi, T., Banba, M., Umehara, Y., Kouchi, H., Izui, K. et al. (2003) Characterization and expression analysis of genes encoding phosphoenolpyruvate carboxylase and phosphoenolpyruvate carboxylase kinase of *Lotus japonicus*, a model legume. *Molecular Plant–Microbe Interactions®*, 16, 281–288. Available from: https://doi.org/10.1094/MPMI.2003.16.4.281

Palmieri, L., Picault, N., Arrigoni, R., Besin, E., Palmieri, F. & Hodges, M. (2008) Molecular identification of three *Arabidopsis thaliana* mitochondrial dicarboxylate carrier isoforms: organ distribution, bacterial expression, reconstitution into liposomes and functional characterization. *Biochemical Journal*, 410, 621–629. Available from: https://doi.org/10.1042/BJ20070867

Palmieri, L., Santoro, A., Carrari, F., Blanco, E., Nunes-Nesi, A., Arrigoni, R. et al. (2008) Identification and characterization of ADNT1, a novel mitochondrial adenine nucleotide transporter from Arabidopsis. *Plant Physiology*, 148, 1797–1808. Available from: https://doi.org/10.1104/pp.108.130310

Perez-Riverol, Y., Bai, J., Bandla, C., García-Seisdedos, D., Hewapathirana, S., Kamatchinathan, S. et al. (2022) The PRIDE database resources in 2022: a hub for mass spectrometry-based proteomics evidences. *Nucleic Acids Research*, 50, D543–D552. Available from: https://doi.org/10.1093/nar/gkab1038

Ralser, M., Wamelink, M.M., Kowald, A., Gerisch, B., Heeren, G., Struys, E.A. et al. (2007) Dynamic rerouting of the carbohydrate flux is key to counteracting oxidative stress. *Journal of Biology*, 6, 10. Available from: https://doi.org/10.1186/jbiol61

Rawsthorne, S. & Larue, T.A. (1986) Preparation and properties of mitochondria from cowpea nodules. *Plant Physiology*, 81, 1092–1096. Available from: https://doi.org/10.1104/pp.81.4.1092

Reddy, P.M., Kouchi, H. & Ladha, J.K. (1998) Isolation, analysis and expression of homologues of the soybean early nodulin gene GmENOD93 (GmN93) from rice. *Biochimica et Biophysica Acta (BBA) – Gene Structure and Expression*, 1443, 386–392. Available from: https://doi.org/10.1016/S0167-4781(98)00232-2

Reiter, L., Rinner, O., Picotti, P., Hüttenhain, R., Beck, M., Brusniak, M.-Y. et al. (2011) mProphet: automated data processing and statistical validation for large-scale SRM experiments. *Nature Methods*, 8, 430–435. Available from: https://doi.org/10.1038/nmeth.1584

Rimmer, K.A., Foo, J.H., Ng, A., Petrie, E.J., Shilling, P.J., Perry, A.J. et al. (2011) Recognition of mitochondrial targeting sequences by the import receptors Tom20 and Tom22. *Journal of Molecular Biology*, 405, 804–818. Available from: https://doi.org/10.1016/j.jmb.2010.11.017

Ritchie, M.E., Phipson, B., Wu, D., Hu, Y., Law, C.W., Shi, W. et al. (2015) limma powers differential expression analyses for RNA-sequencing and microarray studies. *Nucleic Acids Research*, 43, e47. Available from: https://doi.org/10.1093/nar/gkv007

Robinson, M.D., McCarthy, D.J. & Smyth, G.K. (2010) edgeR: a bioconductor package for differential expression analysis of digital gene expression data. *Bioinformatics*, 26, 139–140. Available from: https://doi.org/10.1093/bioinformatics/btp616

Rocha, M., Sodek, L., Licausi, F., Hameed, M.W., Dornelas, M.C. & Van Dongen, J.T. (2010) Analysis of alanine aminotransferase in various organs of soybean (*Glycine max*) and in dependence of different nitrogen fertilisers during hypoxic stress. *Amino Acids*, 39, 1043–1053. Available from: https://doi.org/10.1007/s00726-010-0596-1

Rosendahl, L., Dilworth, M.J. & Glenn, A.R. (1992) Exchange of metabolites across the peribacteroid membrane in pea root nodules. *Journal of Plant Physiology*, 139, 635–638. Available from: https://doi.org/10.1016/S0176-1617(11)80385-8

Rugen, N., Senkler, M. & Braun, H.-P. (2023) Deep proteomics reveals incorporation of unedited proteins into mitochondrial protein complexes in Arabidopsis. *Plant Physiology*, 195, 1180–1199. Available from: https://doi.org/10.1093/plphys/kiad655

Schulte, C.C.M., Borah, K., Wheatley, R.M., Terpolilli, J.J., Saalbach, G., Crang, N. et al. (2021) Metabolic control of nitrogen fixation in rhizobium-legume symbioses. *Science Advances*, 7, eabh2433. Available from: https://doi.org/10.1126/sciadv.abh2433

Schulze, J., Tesfaye, M., Litjens, R.H.M.G., Bucciarelli, B., Trepp, G., Miller, S. et al. (2002) Malate plays a central role in plant nutrition. In: Horst, W.J., Bürkert, A., Claassen, N., Flessa, H., Frommer, W.B., Goldbach, H. et al. (Eds.) *Progress in plant nutrition: plenary lectures of the XIV International Plant Nutrition Colloquium*. Dordrecht: Springer, pp. 133–139. https://doi.org/10.1007/978-94-017-2789-1_10

Smith, P.M.C. & Atkins, C.A. (2002) Purine biosynthesis. big in cell division, even bigger in nitrogen assimilation. *Plant Physiology*, 128, 793–802. Available from: https://doi.org/10.1104/pp.010912

Song, J., Herrmann, J.M. & Becker, T. (2021) Quality control of the mitochondrial proteome. *Nature Reviews Molecular Cell Biology*, 22, 54–70. Available from: https://doi.org/10.1038/s41580-020-00300-2

Streeter, J.G. (1987) Carbohydrate, organic acid, and amino acid composition of bacteroids and cytosol from soybean nodules. *Plant Physiology*, 85, 768–773. Available from: https://doi.org/10.1104/pp.85.3.768

Sun, F., Suen, P.K., Zhang, Y., Liang, C., Carrie, C., Whelan, J. et al. (2012) A dual-targeted purple acid phosphatase in *Arabidopsis thaliana* moderates carbon metabolism and its overexpression leads to faster plant growth and higher seed yield. *New Phytologist*, 194, 206–219. Available from: https://doi.org/10.1111/j.1469-8137.2011.04026.x

Sun, Y., Xie, M., Xu, Z., Chan, K.C., Zhong, J.Y., Fan, K. et al. (2020) Differential RNA editing and intron splicing in soybean mitochondria during nodulation. *International Journal of Molecular Sciences*, 21, 9378. Available from: https://doi.org/10.3390/ijms21249378

Tajima, S. (2004) Ureide biosynthesis in legume nodules. *Frontiers in Bioscience*, 9, 1374. Available from: https://doi.org/10.2741/1345

Takanashi, K., Takahashi, H., Sakurai, N., Sugiyama, A., Suzuki, H., Shibata, D. et al. (2012) Tissue-specific transcriptome analysis in nodules of *Lotus japonicus*. *Molecular Plant–Microbe Interactions®*, 25, 869–876. Available from: https://doi.org/10.1094/MPMI-01-12-0011-R

Thal, B., Braun, H.-P. & Eubel, H. (2018) Proteomic analysis dissects the impact of nodulation and biological nitrogen fixation on *Vicia faba* root nodule physiology. *Plant Molecular Biology*, 97, 233–251. Available from: https://doi.org/10.1007/s11103-018-0736-7

Thumfort, P.P., Layzell, D.B. & Atkins, C.A. (1999) Diffusion and reaction of oxygen in the central tissue of ureide-producing legume nodules. *Plant, Cell & Environment*, 22, 1351–1363. Available from: https://doi.org/10.1046/j.1365-3040.1999.00498.x

Thumuluri, V., Almagro Armenteros, J.J., Johansen, A.R., Nielsen, H. & Winther, O. (2022) DeepLoc 2.0: multi-label subcellular localization prediction using protein language models. *Nucleic Acids Research*, 50, W228–W234. Available from: https://doi.org/10.1093/nar/gkac278

Ting, Y.S., Egertson, J.D., Payne, S.H., Kim, S., MacLean, B., Käll, L. et al. (2015) Peptide-centric proteome analysis: an alternative strategy for the analysis of tandem mass spectrometry data. *Molecular & Cellular Proteomics*, 14, 2301–2307. Available from: https://doi.org/10.1074/mcp.O114.047035

De La Torre, F., Canas, R.A., Pascual, M.B., Avila, C. & Canovas, F.M. (2014) Plastidic aspartate aminotransferases and the biosynthesis of essential amino acids in plants. *Journal of Experimental Botany*, 65, 5527–5534. Available from: https://doi.org/10.1093/jxb/eru240

Traba, J., Satrústegui, J. & del Arco, A. (2009) Characterization of SCaMC-3-like/slc25a41, a novel calcium-independent mitochondrial ATP-Mg/Pi carrier. *Biochemical Journal*, 418, 125–133. Available from: https://doi.org/10.1042/BJ20081262

Trepp, G.B., Plank, D.W., Stephen Gantt, J. & Vance, C.P. (1999) NADH-glutamate synthase in alfalfa root nodules. Immunocytochemical localization. *Plant Physiology*, 119, 829–838. Available from: https://doi.org/10.1104/pp.119.3.829

Trepp, G.B., Temple, S.J., Bucciarelli, B., Shi, L.F. & Vance, C.P. (1999) Expression map for genes involved in nitrogen and carbon metabolism in alfalfa root nodules. *Molecular Plant–Microbe Interactions®*, 12, 526–535. Available from: https://doi.org/10.1094/MPMI.1999.12.6.526

Tyanova, S., Temu, T. & Cox, J. (2016) The MaxQuant computational platform for mass spectrometry-based shotgun proteomics. *Nature*

Protocols, 11, 2301–2319. Available from: https://doi.org/10.1038/nprot.2016.136

Valderrama-Martín, J.M., Ortigosa, F., Ávila, C., Cánovas, F.M., Hirel, B., Cantón, F.R. et al. (2022) A revised view on the evolution of glutamine synthetase isoenzymes in plants. *The Plant Journal*, 110, 946–960. Available from: https://doi.org/10.1111/tpj.15712

Vanlerberghe, G. (2013) Alternative oxidase: a mitochondrial respiratory pathway to maintain metabolic and signaling homeostasis during abiotic and biotic stress in plants. *International Journal of Molecular Sciences*, 14, 6805–6847. Available from: https://doi.org/10.3390/ijms14046805

Voon, C.P., Law, Y.-S., Guan, X., Lim, S.-L., Xu, Z., Chu, W.-T. et al. (2021) Modulating the activities of chloroplasts and mitochondria promotes adenosine triphosphate production and plant growth. *Quantitative Plant Biology*, 2, e7. Available from: https://doi.org/10.1017/qpb.2021.7

Wang, Q., Yung, W.-S., Wang, Z. & Lam, H.-M. (2020) The histone modification H3K4me3 marks functional genes in soybean nodules. *Genomics*, 112, 5282–5294. Available from: https://doi.org/10.1016/j.ygeno.2020.09.052

Wang, Y., Carrie, C., Giraud, E., Elhafez, D., Narsai, R., Duncan, O. et al. (2012) Dual location of the mitochondrial preprotein transporters B14.7 and Tim23-2 in complex I and the TIM17:23 complex in *Arabidopsis* links mitochondrial activity and biogenesis. *The Plant Cell*, 24, 2675–2695. Available from: https://doi.org/10.1105/tpc.112.098731

Wang, Y., Zhang, P., Li, L., Li, D., Liang, Z., Cao, Y. et al. (2022) Proteomic analysis of alfalfa (*Medicago sativa* L.) roots in response to rhizobium nodulation and salt stress. *Genes*, 13, 2004. Available from: https://doi.org/10.3390/genes13112004

Waters, J.K., Hughes, B.L., Purcell, L.C., Gerhardt, K.O., Mawhinney, T.P. & Emerich, D.W. (1998) Alanine, not ammonia, is excreted from N_2-fixing soybean nodule bacteroids. *Proceedings of the National Academy of Sciences*, 95, 12038–12042. Available from: https://doi.org/10.1073/pnas.95.20.12038

Waters, J.K., Mawhinney, T.P. & Emerich, D.W. (2020) Nitrogen assimilation and transport by *ex planta* nitrogen-fixing *Bradyrhizobium diazoefficiens* bacteroids is modulated by oxygen, bacteroid density and L-malate. *International Journal of Molecular Sciences*, 21, 7542. Available from: https://doi.org/10.3390/ijms21207542

SUPPORTING INFORMATION

Additional supporting information can be found online in the Supporting Information section at the end of this article.

How to cite this article: Sin, W.-C., Liu, J., Zhong, J. Y., Lam, H.-M. & Lim, B. L. (2024) Comparative proteomics analysis of root and nodule mitochondria of soybean. *Plant, Cell & Environment*, 1–18. https://doi.org/10.1111/pce.15026